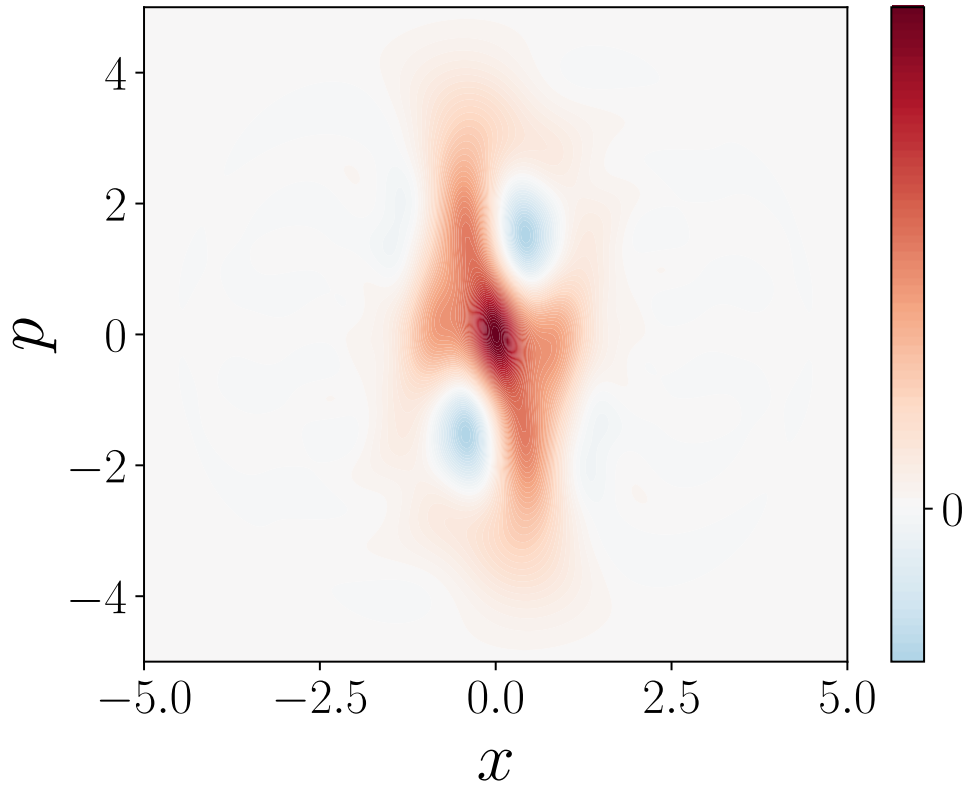

On generating propagating grid states from superconducting circuits

Master's thesis in Physics

ALBIN EDENMYR

DEPARTMENT OF MICROTECHNOLOGY AND NANOSCIENCE

CHALMERS UNIVERSITY OF TECHNOLOGY
Gothenburg, Sweden 2024
www.chalmers.se

Master's thesis 2024

On generating propagating grid states from superconducting circuits

Albin Edenmyr

CHALMERS
UNIVERSITY OF TECHNOLOGY

Department of Microtechnology and Nanoscience
Applied Quantum Physics Laboratory
Chalmers University of Technology
Gothenburg, Sweden 2024

On generating propagating grid states from superconducting circuits
ALBIN EDENMYR

Supervisor: Maryam Khanahmadi
Examiner: Göran Johansson

Master's Thesis 2024
Department of Microtechnology and Nanoscience
Applied Quantum Physics Laboratory
Chalmers University of Technology
SE-412 96 Gothenburg
Telephone +46 31 772 1000

Cover: Wigner function of traveling state after our preparation scheme. We note that this is not an adequate GKP state, but that it does contain negativity.

Typeset in LaTeX
Printed by Chalmers Reproservice
Gothenburg, Sweden 2024

On generating propagating grid states from superconducting circuits
ALBIN EDENMYR
Department of Microechnology and Nanoscience
Chalmers University of Technology

Abstract

Due to current advancements in quantum technologies, quantum processors are growing in size, and we enter into the distributed quantum computing era. Distributed quantum computing is based on sharing information between several spatially distributed processors. This is achieved by sending photons carrying the quantum information between two or more distant quantum processors.

Since we want all communication to be secure and tolerant against unavoidable noise in the communication channel, one attractive possibility is to encode the quantum information in error correctable quantum states, e.g. GKP states, Schrödinger cat states. The goal with error correctable states is to compensate for errors and loss in our communication channels.

Previously it has been shown that optional encoding of quantum information from a processor into a quantum propagating mode makes the output field multimode, i.e. it consists of a combination of single mode states with different temporal envelopes.

As a solution to this problem, we study the generation of error correctable quantum states, specifically GKP states, in highly lossy quantum circuits to prepare it as a traveling state in a waveguide instead of in the system. In this thesis, we present the basic theory for the preparation protocol; optimal release and the necessary extensions to compensate for noise. We study the character of the output field, as well as restrictions of this methodology.

Keywords: distributed quantum computing, GKP states, input-output theory, propagating quantum state.

Acknowledgements

I want to thank my supervisor Maryam Khanahmadi for all the help and guidance during the project. Your support has been invaluable and our discussions have always been very fruitful. Having such an interested supervisor has been very motivating and fun.

I also want to thank my examiner Göran Johansson, for helping me find a project that I would find interesting, and for always taking time to answer questions when they arise.

Albin Edenmyr, Gothenburg, June 2024

Contents

1
Introduction

1.1 Distributed quantum computing

Quantum technologies have advanced at a rapid speed in recent years, both in the theoretical and experimental departments. This has allowed us to control quantum states, and has given researchers hope that quantum computers can be realized and used to solve real world problems.

One of the main challenges of quantum computation is how to design a quantum computer such that noise levels and decoherence is suppressed, both on the level of individual computational units as well as for overarching chip architectures.

One aspect of the problem is that qubits have cross-talk. In certain cases this is desirable and highly necessary in order to have inter-qubit information exchange, while in other cases it leads to disturbances. With increased size of quantum computers, the unwanted talk between qubits becomes harder and harder to keep track off, and therefore hard to counteract. Through advances in quantum engineering, these cross-talk noise levels are being reduced, but there is still need for improvements.

One possible solution to this problem is through distributed quantum computing. This means that the main computation unit is split into several parts, which are spatially distributed. These sub-components are then used as a cluster to solve computational tasks. This limits the effects of cross-talk to qubits within the same sub-component of the quantum computer. Since these errors tend to scale with the size of the system, this gives a cap to the errors that might arise. In order for these systems to work together, there is a need for communication between them. In particular, quantum information has to be sent and received in a stable manner. Quantum information is vulnerable, especially in regards to measurements and errors via interactions with the environment. In order to secure the state information traveling between the quantum circuits, this information transfer has to be done with error correctable states, i.e. states that are resistant to errors. Some examples of error correcting states are Schrödinger cat states and GKP states.

1.2 Motivation and goal

In this thesis we will concern ourselves with GKP states. They have interesting error correction properties, but have proven to be challenging to produce in a deterministic manner (without the need for e.g. measurements). Recently, a scheme for deterministic generation of stationary GKP states, i.e. GKP states stabilized in

a circuit, has been presented [1]. For communication purposes, a stationary state is not very helpful, since the information is not going anywhere, but the proposed deterministic generation scheme is interesting as a building block. Therefore, this preparation scheme is a starting point for attempts at generating flying GKP states.

This thesis explores emission of GKP states by following this generation scheme in a circuit which is strongly coupled to a waveguide, allowing the state to leak out, while also considering the multimode character of the emitted state [2]. This work is entirely theoretical, and is based on simulations in QuTiP [3, 4]. The preparation scheme is combined with a method for dealing with emitted states and the corresponding waveguide modes [5, 6].

1.3 Overview of thesis

With the goal of ending up with simulated flying GKP states in a waveguide, we begin with a thorough orientation through the relevant theory in Chapter 2. We introduce the basics of quantum computation and the theory for working with systems with loss present, introducing the Lindblad master equation for solving time dynamics. We move on to a discussion on error correction and an introduction to GKP states as well as how to stabilize them in a cavity. In order to deal with the emitted state in an efficient way, Chapter 3 is dedicated to covering input-output theory, as well as its formulation when the inputs and outputs are pulses. We also introduce the SLH formalism, a way of compressing networks of many subsystems into a full system, which is easier to simulate. We talk about how to leak GKP states by coupling the system to a waveguide. Chapter 3 also covers shortcuts to adiabaticity, a way to decrease preparation times and therefore limit the time errors can act.

Moving on, Chapter 4 presents the results of our simulations. We generate stationary GKP states, and add shortcuts to adiabaticity, which severely deteriorates the quality of the GKP state. We then open the system and simulate the full system state generation. We see that we can achieve Wigner negativity for certain parameter values, and we study the multimodeness of the emitted state.

Chapter 5 contains a summary of the thesis and some conclusions, as well as an indication of what future work is needed.

2
Theory

This chapter will describe the relevant theory for the project. We start with a short introduction to qubits, the smallest building block of a quantum computer. Since errors are present in all physical systems, and especially prevalent in quantum mechanical setups, we need to deal with noise and correct errors. We model this by introducing a mathematical theory for dealing with open quantum systems, and then talk about error correction. One type of error correctable states are the GKP states, which we introduce and present a state generation scheme for, which will be important in later sections. Through all derivations and calculations, $\hbar = 1$ is assumed.

2.1 Qubits

Quantum computers are the focus of a lot of research. They were first conceptualized by Feynman in 1982 as tools for simulating quantum mechanical systems [7]. Today, quantum computers are believed to be able to solve several other types of problems faster than classical computers, for example certain optimization problems [8]. The core difference between quantum computers and classical computers is the basic computing unit. In the classical case, the smallest logical component of the computer is the *bit*, carrying either the value 0 or 1. The quantum equivalent, the *qubit* (quantum bit), is defined with the same basis, with the two basis states $|0\rangle$ and $|1\rangle$, written in the usual bra-ket notation of quantum mechanics [9]. However, since the qubit is a quantum mechanical entity, it can also be in a superposition of its basis states, i.e.

$$|\psi\rangle = \alpha\,|0\rangle + \beta\,|1\rangle\,, \tag{2.1}$$

where $|\psi\rangle$ denotes the state of the qubit. Here, α and β are complex coefficients, with the condition $|\alpha|^2 + |\beta|^2 = 1$ as our condition for conservation of probability. This can equivalently be expressed in terms of angles as

$$|\psi\rangle = e^{i\xi}\left(\cos\left(\frac{\theta}{2}\right)|0\rangle + e^{i\phi}\sin\left(\frac{\theta}{2}\right)|1\rangle\right). \tag{2.2}$$

We can safely disregard the global phase ξ, since this will not affect the dynamics of the qubit state in any way. This leaves us with two angles as independent variables. We can map this to a sphere, referred to as the *Bloch sphere*, shown in Fig. 2.1.

The main advantage of working with qubits rather than bits is the exponential increase of the size of the Hilbert space when working with several qubits. With N qubits, the Hilbert space will have 2^N dimensions, which can be utilized in quantum

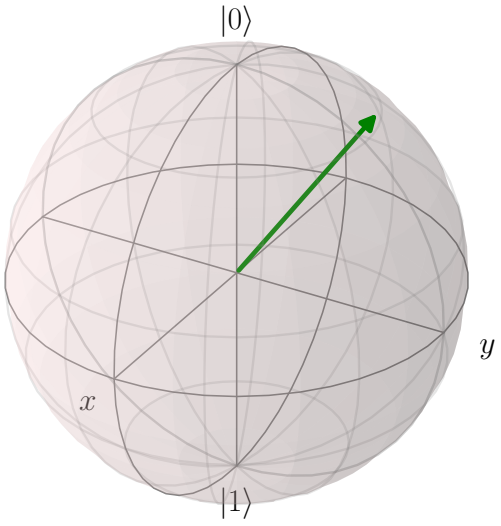

Fig. 2.1: Bloch sphere representation of pure quantum state. Ground ($|0\rangle$) and excited state ($|1\rangle$) are located at north and south pole respectively. The state is represented by the arrow and can point to any point on the perimeter of the sphere. In this example we are more likely to measure $|0\rangle$ than $|1\rangle$.

algorithms to achieve speedups. In the end of a calculation, the result will have to be measured, leading to a collapse of the state. Each qubit will be reduced to either $|0\rangle$ or $|1\rangle$, with the probabilities $|\alpha|^2$ and $|\beta|^2$ respectively.

2.2 Open Quantum Systems

In physical systems, it is impossible to isolate the desired system from the environment. For example, in experimental setups this is obvious since one needs to measure the result of the experiments. The measurement instruments will then by necessity interact with the system, and will thus affect the system. In other cases, it is possible to lose photons to the environment, to have energy dissipation through heat transfer, or phase decoherence by interaction with environment fields, as well as other processes.

In order to model systems in a realistic way, this has to be taken into account. The resulting theory is the theory of open quantum systems, as opposed to closed quantum systems. In an open system, the bra-ket description of the quantum states fails, and instead one has to deal with ensembles of states.

2.2.1 Density matrix formalism

In a closed system setting, quantum states can be represented by state vectors, typically written in the bra-ket notation. The nature of these states is probabilistic in the way that observing an observable of the state will collapse it into an eigenstate of the observable in a probabilistic manner. This randomness is purely quantum mechanical, and states with only this source of randomness are referred to as *pure*

states. For an open system, the same notation cannot be used. This is because the environment will give rise to a mixture of states in the system, meaning that the states in different repetitions of the experiments might differ from each other due to these interactions. This is referred to as *mixed state*. A mixed state can generally be viewed as a average over several pure states, but with lost phase relations between the individual states.

Mixed states cannot be written as state vectors, giving rise to the alternative notation of density matrices. A density matrix describes the full quantum state in an ensemble, taking into account both the quantum randomness and the randomness coming from the distribution in the ensemble. It is defined in terms of state vectors as

$$\rho = \sum_i p_i \left|\psi_i\right\rangle \left\langle\psi_i\right|, \tag{2.3}$$

where p_i is the probability of the state being in $|\psi_i\rangle$.

To calculate the expectation value for a mixed state described by the density operator ρ, the formula

$$\langle\hat{O}\rangle = \mathrm{Tr}\left[\hat{O}\rho\right] \tag{2.4}$$

is useful [10, 11].

2.2.2 Master equation

The time dynamics of a state vector (pure state) is determined by the Schrödinger equation

$$i\partial_t \left|\psi\right\rangle = \mathcal{H}\left|\psi\right\rangle. \tag{2.5}$$

For the density matrix, we wish to find a similar equation of motion. We start with taking the time derivative of one term of the density operator, $\rho_i = p_i \left|\psi_i\right\rangle \left\langle\psi_i\right|$,

$$\partial_t \rho_i = \partial_t p_i \left|\psi_i\right\rangle \left\langle\psi_i\right| = p_i \left(\partial_t \left|\psi_i\right\rangle\right) \left\langle\psi_i\right| + \left|\psi_i\right\rangle \left(\partial_t \left\langle\psi_i\right|\right). \tag{2.6}$$

We can now utilize the Schrödinger equation and its conjugate to get

$$\partial_t \rho_i = -i\mathcal{H} p_i \left|\psi_i\right\rangle \left\langle\psi_i\right| + i\mathcal{H} p_i \left|\psi_i\right\rangle \left\langle\psi_i\right| = -i[\mathcal{H}, \rho_i]. \tag{2.7}$$

Because of the linearity of the equation, it holds for the full density matrix as well,

$$\partial_t \rho = -i[\mathcal{H}, \rho]. \tag{2.8}$$

This is known as the Liouville-von Neumann equation [10, 11]. Much like the Schrödinger equation, this holds for closed systems. To make it more general, dissipator terms are added to the right hand side of the equation. For a derivation of how this is done, we refer to [9]. The result is the Lindblad master equation

$$\partial_t \rho = -i[\mathcal{H}, \rho] + \sum_k \mathcal{D}[L_k]\rho, \tag{2.9}$$

where k is the index for different loss mechanisms and $\mathcal{D}[L_k]$ is a superoperator describing the loss mechanism, dependent on the loss operator L_k, with an implicit loss rate typically denoted by γ_k. The superoperator can be expanded as

$$\mathcal{D}[L_k] = L_k \rho L_k^\dagger - \frac{1}{2}\left\{L_k^\dagger L_k, \rho\right\}, \tag{2.10}$$

where $\{\cdot,\cdot\}$ denotes the anti-commutator.

We will work with bosonic systems, and restrict ourselves to only dealing with one loss mechanism, photon loss. This restriction is valid since photon loss is the main coupling mechanism for bosonic systems [12]. In this case the master equation is reduced to

$$\partial_t \rho = -i[\mathcal{H}, \rho] + \gamma a \rho a^\dagger - \frac{\gamma}{2}\left\{a^\dagger a, \rho\right\}, \tag{2.11}$$

where $a, a^\dagger$ are the annihilation and creation operators for the system, and γ is the photon loss rate.

2.2.3 Wigner functions and state visualization

A useful tool for visualizing continuous variable quantum states is the Wigner function [13]. The Wigner function relates a density matrix to its phase space distribution, where phase space is the space spanned by the quadrature variables x and p, i.e. position and momentum. For a classical particle, the phase space would have a single point characterizing the state, since simultaneous knowledge on the particle's position and momentum is allowed. However, quantum mechanics forbids this, since the two quadratures are non-commuting operators. Instead, the phase space representation of a quantum state has to consist of some distribution. One such distribution is the Wigner function, a so-called quasi-probability distribution. In many ways it is like a probability distribution, but one crucial difference is that it can take negative values. The negativity of the Wigner function is a measure of non-classicality, and is a topic of much interest for researchers [14–18].

The Wigner function is defined as

$$W(q,p) = \frac{1}{2\pi}\int_{-\infty}^{\infty} \langle q + x/2|\rho|q - x/2\rangle\, e^{ipx} dx, \tag{2.12}$$

where $|q \pm x/2\rangle$ are eigenstates of the position operator [19]. It is invertible, meaning that we have a one-to-one relation between the density matrix and the Wigner function [20, 21]. This means that by studying the Wigner function, we gain all knowledge we need to recreate the density matrix. By integrating the Wigner function over one of the two quadratures, the remaining marginal distribution is an ordinary probability distribution. Some examples of Wigner functions are shown in Fig. 2.2.

2.3 Error correction

We have now seen methods for modeling the noise. For any real application, this is obviously not enough, we also need to correct for it. We will have unwanted couplings to the environment, which acts stochastically on the system. For quantum computation, this means trouble, since unwanted alteration to the quantum states used for calculations gives erroneous results [22, 23]. As in the classical counterpart, errors are mitigated through error correction schemes. The goal of an error correction scheme is to be able to non-destructively measure whether or not an error has

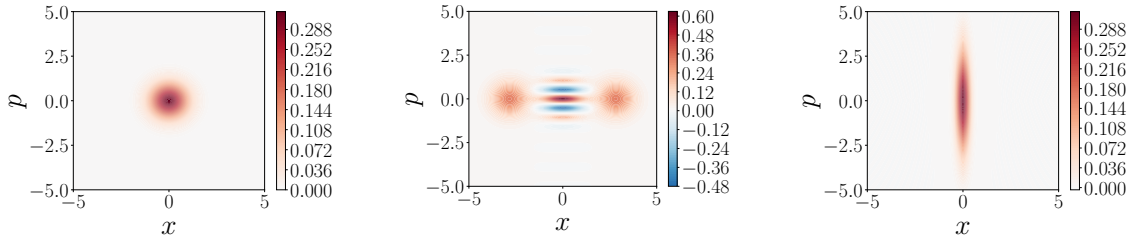

(a) Vacuum state, minimum uncertainty centered at origin of phase space.

(b) Cat state, the superposition of two coherent states. This showcases Wigner negativity and is therefore strictly non-classical.

(c) Squeezed state, in this case squeezed in the x quadrature. The uncertainty principle is not broken, since the state expands in the other quadrature.

Fig. 2.2: Three examples of basic Wigner functions.

occurred, and subsequently correct the error. This is based in redundantly encoding the information in the state.

For a discrete qubit system, simple examples of error correction codes are the bit-flip or phase-flip codes [22, 23]. Taking the example of the bit flip code, it encodes the logical qubit states into sets of three as

$$|0\rangle_{\mathrm{L}} = |000\rangle \tag{2.13}$$
$$|1\rangle_{\mathrm{L}} = |111\rangle\,. \tag{2.14}$$

So far, this looks similar to classical repetition codes. The main difference is that we cannot measure the individual qubits in order to do a majority vote for the logical state. Since the quantum state will collapse upon direct measurement, this is not an option to detect the error. Instead, stabilizer measurements are used. The *stabilizers* of the state is the set of operators $\hat{O}$ for which $\hat{O}\,|\psi\rangle = |\psi\rangle$ [22].

Consider a bit flip error occurring on the third qubit of our logical states, the states are changed as

$$|000\rangle \to |001\rangle \tag{2.15}$$
$$|111\rangle \to |110\rangle\,. \tag{2.16}$$

In the case of the bit-flip code, the operators Z_1Z_2 and Z_2Z_3 are stabilizers, where Z is the Pauli Z gate,

$$Z = \begin{pmatrix} 1 & 0 \\ 0 & -1 \end{pmatrix}, \tag{2.17}$$

and the subscript denotes which qubit the operator acts on. This can be seen through direct calculation on the states $|abc\rangle$, where a, b, c can take values 0 or 1 (in Eq. (2.15) $a = 0, b = 0, c = 1$).

$$Z_1Z_2\,|abc\rangle = Z_1(-1)^b\,|abc\rangle = (-1)^{a+b}\,|abc\rangle \tag{2.18}$$
$$Z_2Z_3\,|abc\rangle = Z_2(-1)^c\,|abc\rangle = (-1)^{b+c}\,|abc\rangle\,. \tag{2.19}$$

We can see that before the error has occurred, $a+b$ and $b+c$ will always be positive, leaving the state unchanged by the stabilizers, but if an error has occurred on our third qubit, the $b+c$ will be odd, giving us a global phase factor on the state. By this non-projective measurement, we can conclude that an error has occurred, where it has occurred, and we can correct it. The same stabilizers work for identifying errors on the first and second qubit as well.

Another very useful quantum property for error correction is that since we can have arbitrary rotations $R_3(\theta)$ around the Bloch sphere, not every error will take us from $|0\rangle$ to $|1\rangle$. We could have errors of arbitrary rotations. This is not an issue with the three qubit bit-flip code, since the stabilizer measurements will project the state as

$$R_3(\theta)\,|000\rangle \rightarrow \begin{cases} |000\rangle \\ |001\rangle\,, \end{cases} \tag{2.20}$$

from which the error correction works as described above [23]. This is one type of error syndrome and its resolution, which holds for a bit-flip on any location. The phase-flip code works in a similar way.

For continuous variable quantum computing, it gets slightly more involved. Since there is a continuum of states, small shifts in the quantum state will have a larger impact on measured observables. The current way around this problem is by encoding a discrete basis in a continuous state. There are several ways of doing this, some of the most prominent examples being the cat codes and the GKP encoding, which we will focus on in this work [24].

2.4 GKP states

The GKP scheme, where an infinite-dimensional state is used to encode a finite-dimensional logical state used for computation, was first introduced in 2001 by Gottesman, Kitaev and Preskill (GKP) [25]. For an extensive review of state-of-the-art GKP research we refer to [26].

2.4.1 Ideal GKP states

The main idea of bosonic error correction is to encode a discrete system in a continuous one. Unlike the qubit/qudit system, the continuous system has continuous errors, a slight shift in the state will have notable effect on the observables. In the Wigner space, this can be seen as a shift in the state quadratures, which we need to account for and correct. In the ideal case, we would like a very narrow peak in phase space to be able to shift the state as precisely as possible. However, due to the uncertainty principle, it is unphysical to have small variances in both quadratures simultaneously. The GKP encoding surmounts this problem by introducing a grid of delta peaks instead of a single one, which allows for narrow peaks while having a large variance. They are therefore referred to as *grid states*. This solves our problem with the uncertainty principle while still letting us use narrow peaks for error correction.

The GKP logical states (code-words) are defined as

$$|+\rangle_{\text{GKP}} = \sum_{s=-\infty}^{\infty} |2n\sqrt{\pi}\rangle_q \tag{2.21}$$

$$|-\rangle_{\text{GKP}} = \sum_{s=-\infty}^{\infty} |(2n+1)\sqrt{\pi}\rangle_q \,, \tag{2.22}$$

where $|\cdot\rangle_q$ denotes the infinitely q-squeezed position eigenstates [26]. The code-words could instead be expressed in terms of infinitely squeezed momentum eigenstates.

The logical states of this encoding is shown in Fig. 2.3. It is clear that shifting the state by $\sqrt{\pi}$ along the q quadrature will correspond to a transform between the $|+\rangle_{\text{GKP}}$ and $|-\rangle_{\text{GKP}}$ GKP states, i.e. it corresponds to our logical X gate. This distance between the peaks is chosen such that the commutation relations become $[x, p] = i$. For further details of the encoding, its logical operations and commutation relations, we refer to [25].

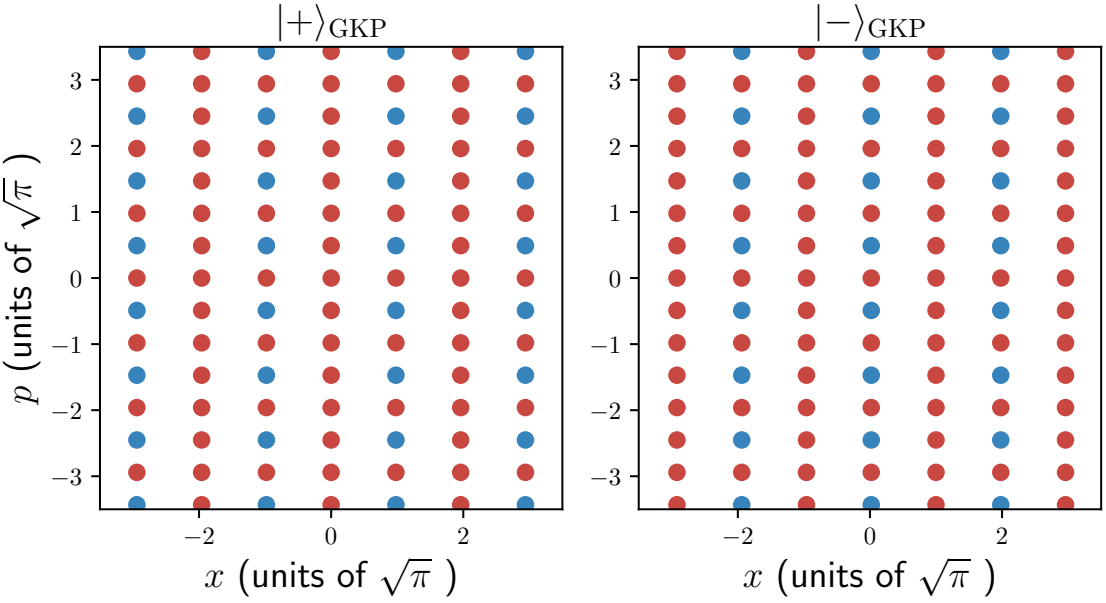

Fig. 2.3: Wigner plot of ideal GKP states. Red (blue) dots correspond to positive (negative) Dirac delta peaks.

As in the case of the bit-flip code in the discrete variable case, errors in the GKP setting are corrected by stabilizer measurements, which are defined as

$$S_1 = \exp\left(\sqrt{2\pi/n}ix\right) \tag{2.23}$$

$$S_2 = \exp\left(-\sqrt{2\pi/n}ip\right). \tag{2.24}$$

These can deal with both small and large shifts in either quadrature [25].

There are several other types of GKP states beyond the square grid GKP state. For example, the hexagonal GKP states and magic GKP states, which both have different Wigner space configurations. The error correction capabilities of these states are analogous to the square GKP state.

2.4.2 Approximated GKP states

It is clear that having grid states extending to infinity in both quadratures consisting of delta peaks is not physical, since it requires infinite energy. In order to implement GKP states, approximations have to be made. This is done by first limiting the extension of the GKP states in phase space by applying some Gaussian to the ideal GKP states, attenuating the peaks far from the origin. The delta peaks are then replaced by narrow Gaussians centered on the same points. The approximate codewords are defined as

$$|+\rangle_{\text{GKP}} \propto \sum_{s\in\mathbb{Z}} e^{-\frac{(2\sqrt{\pi}s)^2}{2\varepsilon^{-2}}} \hat{D}(s\sqrt{2\pi})\hat{S}_r|\text{vac}\rangle \tag{2.25}$$

$$|-\rangle_{\text{GKP}} \propto \sum_{s\in\mathbb{Z}} e^{-\frac{\left(2\sqrt{\pi}\left(s+\frac{1}{2}\right)\right)^2}{2k^{-2}}} \hat{D}\left(\left(s+\tfrac{1}{2}\right)\sqrt{2\pi}\right)\hat{S}_r|\text{vac}\rangle, \tag{2.26}$$

where we see that we now start from the vacuum state, i.e. a coherent state with zero displacement, which is then squeezed and displaced [25, 27–29].

The peaks of the approximate GKP states will therefore be more spread out in Wigner space compared to the ideal versions. They will also not extend to infinity in either quadrature, as seen in Fig. 2.4. This specific state is a so-called GKP magic state, which can be prepared for example as in [30].

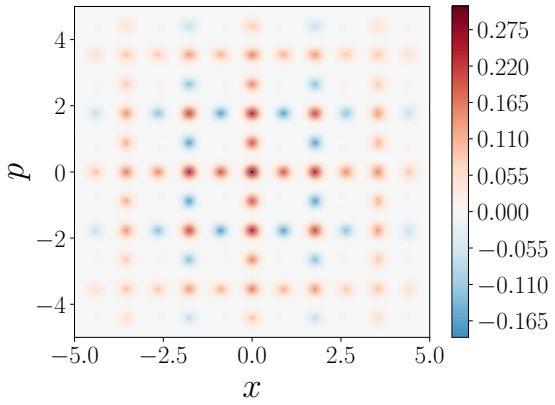

Fig. 2.4: Approximated GKP state. Note that this state is not the same type of GKP as Fig. 2.3. Rather, this is a GKP magic state, generated following [30].

2.4.3 GKP Hamiltonian

Common practice when preparing intricate bosonic states has been to use measurement based preparation protocols. While these methods are sufficient to prepare GKP states, they are not ideal for communication purposes, since the preparation scheme is probabilistic. There are alternative approaches, allowing deterministic generation of GKP states by stabilizing them as ground states of a GKP Hamiltonian. This Hamiltonian is defined as

$$\begin{aligned}\mathcal{H}_{\text{GKP}} &= -\frac{J}{2}\left(D(\sqrt{2\pi}) + D(i\sqrt{2\pi})\right) + \text{H.C.} = \\ &= -J\left(\cos(2\sqrt{\pi}x) + \cos(2\sqrt{\pi}p)\right).\end{aligned} \tag{2.27}$$

It has two almost degenerate ground states, which are approximate GKP magic states $|+\rangle_{\mathrm{GKP}}$ and $|-\rangle_{\mathrm{GKP}}$ [30–33], which is our computational basis, acting as $|0\rangle_{\mathrm{L}}$ and $|1\rangle_{\mathrm{L}}$ in the discrete case [1, 25].

2.5 Deterministic preparation of stationary GKP states

From Section 2.4.3 we know that Eq. (2.27) stabilizes our GKP computational states as its degenerate ground states. For a reliable preparation scheme, we need to construct this Hamiltonian and make sure that we are in the ground state. There is a way of doing this using *adiabatic* Hamiltonian evolution using a time-periodic Hamiltonian [1]. In order to understand the preparation scheme, we first need an understanding of adiabatic dynamics and Floquet theory.

2.5.1 Adiabatic evolution

The adiabatic condition refers to the changes in the Hamiltonian being sufficiently slow in order to retain certain desired qualities. Namely, if our initial state is the ground state of the initial Hamiltonian, the state will continue being the ground state of the evolving Hamiltonian $\mathcal{H}(t)$ [23]. The adiabatically evolving Hamiltonian can be written as

$$\mathcal{H}(t) = (1 - t/t_f)\,\mathcal{H}_0 + t/t_f \mathcal{H}_1, \tag{2.28}$$

where $\mathcal{H}_0$ is the initial Hamiltonian with known ground state, and $\mathcal{H}_1$ is the final Hamiltonian that governs our final system. The adiabatic condition then sets limits on the parameter t_f, i.e. the preparation time.

$$t_f \gg \max_{s\in[0,1]} \frac{|\langle m(s)\,|\partial_s \mathcal{H}(s)|\,n(s)\rangle|}{|E_1(s) - E_0(s)|^2}, \tag{2.29}$$

where $s = t/t_f$ and $|n(s)\rangle, |m(s)\rangle$ are eigenstates of the Hamiltonian $\mathcal{H}(t)$. This assumes that the Hamiltonian can be rewritten as a function of s rather than t [23, 34].

We take some state $|\psi_n(t)\rangle$ that evolve according to the Schrödinger equation

$$\mathcal{H}(t)\,|\psi_n(t)\rangle = i\partial_t\,|\psi_n(t)\rangle\,, \tag{2.30}$$

with the initial condition $|\psi_n(0)\rangle = |n(0)\rangle$, where $|n(t)\rangle$ denotes an eigenvalue of $\mathcal{H}(t)$, i.e. it fulfills the eigenvalue equation

$$\mathcal{H}(t)\,|n(t)\rangle = E_n(t)\,|n(t)\rangle\,. \tag{2.31}$$

The state evolution for adiabatic drive will be

$$|\psi_n(t)\rangle = e^{i\xi_n(t)}\,|n(t)\rangle\,, \tag{2.32}$$

where $\xi(t)$ is the total phase of the state, explicitly written in terms of a *dynamical phase* and a *geometrical phase* (also known as a *Berry phase*) [35–37]

$$\xi_n(t) = -\int_0^t E_n(t')dt' + i\int_0^t \langle n(t')|\partial_t|n(t')\rangle\,. \tag{2.33}$$

We will later see how to relax the adiabatic condition through addition of additional terms in the Hamiltonian, but for the purposes of generating a stationary state, adiabatic evolution is sufficient.

2.5.2 Floquet theory

In several applications there is a need to deal with quantum dynamics where the Hamiltonian is described by a simple Hamiltonian with a small, periodic perturbation, for example in quantum chaos theory, or, for our purposes, generation of GKP states. In such cases, Floquet theory is a useful tool. In our description we will follow [38]. Floquet theory is a theory for dealing with Hamiltonians that have a periodic time-dependence by splitting the Hamiltonian into a time-periodic part (referred to as the *stroboscopic* part), and a part changing within the periods (called the *micromotion*).

In general, given a Hamiltonian $\mathcal{H}(t)$, the time evolution operator is given as

$$U(t) = \exp_+\left(-i\int dt'\mathcal{H}(t')\right), \tag{2.34}$$

where $\exp_+$ denotes time ordering.

The time evolution operator for the stroboscopic part of the Hamiltonian is called the *Floquet operator*, and is defined as

$$F = U(T) = \exp_+\left(-i\int_0^T dt'\mathcal{H}(t')\right), \tag{2.35}$$

where T is the period time. It is evaluated at discrete time intervals of one period. This gives long-time, time-averaged dynamics [39]. The state at times nT, where $n \in \mathbb{Z}$, is then given by

$$|\psi(nT)\rangle = F^n |\psi(0)\rangle . \tag{2.36}$$

Assume we have a Hamiltonian on the form

$$\mathcal{H}(T) = \mathcal{H}_0 + \lambda V \sum_{n=-\infty}^{\infty} \delta(t - nT), \tag{2.37}$$

i.e. a Hamiltonian with repeating delta function perturbations at each period time. The time evolution operator has the property that

$$U(t, 0) = U(t, t')U(t', 0), \tag{2.38}$$

which applied to the Floquet operator gives

$$F = U(T, 0) = U(T, s)U(s, 0) = U(T + \varepsilon, T - \varepsilon)U(T - \varepsilon, \varepsilon), \tag{2.39}$$

where the last equality comes from shifting the entire integration domain by ε. Explicitly, this gives us

$$F = \exp_+\left(-\frac{i}{\hbar}\int_\varepsilon^{T-\varepsilon} dt'\mathcal{H}(t')\right)\exp_+\left(-\frac{i}{\hbar}\int_{T-\varepsilon}^{T+\varepsilon} dt'\mathcal{H}(t')\right). \tag{2.40}$$

The Dirac function drive only acts on the second exponential, where the integration interval is 2ε. ε is assumed to be infinitesimal, meaning that $\mathcal{H}_0$ will not contribute to this term. The first term on the other hand has no delta function kick, and will only have a contribution from the static Hamiltonian, which gives us

$$F = e^{-i\mathcal{H}_0 T/\hbar} e^{-i\lambda V/\hbar}. \tag{2.41}$$

If we are now interested in the state only at full periods, we can find our state

$$|\psi(nT)\rangle = \left(e^{-i\mathcal{H}_0 T/\hbar} e^{-i\lambda V/\hbar}\right)^n |\psi(0)\rangle . \tag{2.42}$$

For finding the state in between periods, the state can be evolved to the closest full period, and then evolved according to the micromotion Hamiltonian for the dnamics in between periods. However, we will find that this is not necessary in this work.

2.5.3 Preparation scheme

The preparation procedure is based of [1]. The idea is to adiabatically evolve the time-periodic Hamiltonian

$$\mathcal{H}(t) = \omega_0 a^\dagger a + J f(t) \cos(2\sqrt{\pi}\hat{x}), \tag{2.43}$$

where $f(t)$ is our kick drive that holds the time dependence. In the ideal case, it is defined as

$$f(t) = \frac{T}{2} \sum_{n=0}^{\infty} \delta(t - nT/4), \tag{2.44}$$

meaning that we have four kicks in each period. The reason for this choice of Hamiltonian becomes clear after looking at the corresponding Floquet operator. Since we have four kicks in what we define as a period, we could equally well find another Floquet operator for a quarter of a period, $\mathcal{F}$ such that $\mathcal{F}^4 = F$. For this operator we get

$$\begin{aligned}
\mathcal{F} &= \exp_+ \left(-i \int_0^{T/4} \omega_0 a^\dagger a + JT/2 \sum_{n=0}^{\infty} \delta(t' - nT/4) \cos(2\sqrt{\pi}\hat{x}) dt' \right) \\
&= \exp_+ \left(-i \int_\varepsilon^{T/4-\varepsilon} \omega_0 a^\dagger a + JT/2 \sum_{n=0}^{\infty} \delta(t' - nT/4) \cos(2\sqrt{\pi}\hat{x}) dt' \right) \\
&\times \exp_+ \left(-i \int_{T/4-\varepsilon}^{T/4+\varepsilon} \omega_0 a^\dagger a + JT/2 \sum_{n=0}^{\infty} \delta(t' - nT/4) \cos(2\sqrt{\pi}\hat{x}) \right) \\
&= \exp_+ \left(-i\omega_0 a^\dagger a \right) \exp_+ \left(-iJT/2 \cos(2\sqrt{\pi}\hat{x}) \right).
\end{aligned} \tag{2.45}$$

From this we can now say that

$$F = \left(\exp_+ \left(-i\omega_0 a^\dagger a \right) \exp_+ \left(-iJT/2 \cos(2\sqrt{\pi}\hat{x}) \right) \right)^4 . \tag{2.46}$$

It is now possible to show that this is equivalent to

$$F = \exp_+ \left(-iT\mathcal{H}_{\mathrm{GKP}} \right). \tag{2.47}$$

This means that as long as we study the system only at times described by the stroboscopic Hamiltonian, i.e. at $t = nT$, the time evolution will follow that of the GKP Hamiltonian [1].

For experimentally realizable drives, it is obvious that we cannot have delta peaks in the drive. With this in mind, we need to modify the time dependent part of the drive, $f(t)$. We do this by writing the Fourier series of the comb of Dirac delta functions, and then truncating it at some N (we will use $N = 4$, higher values would give a closer approximation of the delta function peaks). We get

$$f(t) = 2 + 4\sum_{n=1}^{N} \cos(4n\omega_0 t) \tag{2.48}$$

The preparation scheme in [1] is to evolve the Hamiltonian

$$\mathcal{H}(t) = \omega_0 a^\dagger a + Jf(t)\cos(2\sqrt{\pi}\hat{x}), \tag{2.49}$$

where $f(t)$ now also incorporates factors controlling the adiabatic evolution. Its explicit form is

$$f(t) = A(t)\left(2 + 4\sum_{n=1}^{N} \cos\left(4n\omega(t)t\right)\right), \tag{2.50}$$

where $A(t)$ controls the strength of the drive, and $\omega(t)$ controls the frequency detuning.

For stabilizing the GKP states, both $A(t)$ and $\omega(t)$ can be chosen to be sigmoid functions, $A(t)$ going from 0 to 1, and $\omega(t)$ going from $\omega_0/(1 - \pi \cdot 10^{-3})$.

Since we want a computational basis of GKP states, we need to be able to prepare both our basis states, $|\pm\rangle_{\text{GKP}}$. This is done by choosing which initial state we have in our system. For generating $|+\rangle_{\text{GKP}}$, we choose the initial Fock state $|0\rangle$, and for $|-\rangle_{\text{GKP}}$ we choose the initial Fock state $|2\rangle$.

3

Propagating GKP

With a foundational knowledge of GKP states and how to generate stationary GKP states in a deterministic manner, we can now move on to a proposed preparation scheme for traveling GKP states in a waveguide. In order to do this, we need an introduction to input-output theory, as well as some extensions for dealing with pulsed inputs and outputs to our system. We introduce the SLH formalism, a powerful tool for finding effective operators for a larger network of multiple components. We then use these tools to find a model description of a system releasing a state into a downstream mode.

When emitting states, we tend to speak in terms of output modes. A very interesting aspect of state emission is the distribution among modes, sometimes referred to as the *multimodeness* of the state. In a linear system, one can expect to only populate a single output mode, but in non-linear systems several output modes can be expected to have a photon population [2]. In experimental settings, emission of low-photon states has already been achieved [40, 41], but for emission of GKP states, we need to account for photon populations in higher excited states.

3.1 Input-Output Theory

The input-output formalism of quantum optics is an effective way of describing the interactions of an open quantum system interacting with the environment. The main idea of the theory is to describe the system in terms of inputs from the environment and outputs to the environment. This gives us an effective description of incident signals scattering on the system, which characterizes our system. It was first introduced by Gardiner and Collett [42]. We will derive it starting from the full system-bath Hamiltonian in our rotating frame with frequency ω, following [9, 20, 42].

$$\mathcal{H}_{\text{total}} = \mathcal{H}_{\text{sys}} + \mathcal{H}_{\text{b}} + \mathcal{H}_{\text{int}}, \tag{3.1}$$

where

$$\mathcal{H}_{\text{sys}} = \Delta a^\dagger a \tag{3.2}$$

is the system Hamiltonian assuming that we are working with a two level system, $\Delta = \omega_0 - \omega$ is the detuning between our system frequency and the frequency of our rotating frame. The operator a is a system annihilation operator. Our environment is modeled in terms of an infinite bath of harmonic oscillators

$$\mathcal{H}_{\text{b}} = \int d\omega \omega b^\dagger(\omega) b(\omega), \tag{3.3}$$

where $b(\omega)$ is the annihilation operator of the mode with frequency ω. The bath operators should fulfill the commutation relations $[b(\omega), b^\dagger(\omega')] = \delta(\omega - \omega')$, meaning that interactions between bath modes of different ω are uncorrelated. We model our interaction as the lowest order interaction possible (weak coupling), where we couple one of the quadratures of the system to one of the quadratures of the bath. This gives us some freedom to chose the exact form of our coupling, since we can pick which quadratures to couple. We couple the generalized position of the system to the generalized momenta of the bath, with a coupling strength $\kappa(\omega)$. We get

$$\mathcal{H}_{\text{int}} = i \int d\omega \kappa(\omega)(a + a^\dagger)(b^\dagger(\omega) - b(\omega)) \approx i \int d\omega \kappa(\omega) \left(a b^\dagger(\omega) - a^\dagger b(\omega) \right), \quad (3.4)$$

where we have only kept terms with an equal amount of creation and annihilation operators, since they are the energy conserving ones to the lowest order. The goal now is to find how the system responds to an incoming field b_{in}. We do this by first writing down the Heisenberg equation of motion for the bath operator $b(\omega)$. We get

$$\dot{b}(\omega) = -i\omega b(\omega) + \kappa(\omega) a. \quad (3.5)$$

This can be solved, giving us

$$b(\omega) = e^{-i\omega(t-t_0)} b_0(\omega) + \kappa(\omega) \int_{t_0}^{t} e^{-i\omega(t-t')} a(t') dt', \quad (3.6)$$

where we have defined $b_0(\omega) = b(\omega, t = t_0)$ as an initial condition for the bath. The initial condition should fulfill the same commutation relations, i. e. $[b_0(\omega), b_0(\omega')] = \delta(\omega - \omega')$. We now make the first Markov approximation, meaning that we approximate the coupling as constant, $\kappa(\omega) = \sqrt{\gamma/2\pi}$. This approximation is valid if the coupling is slowly varying. We now define the *in-field* at time t as

$$b_{\text{in}}(t) = \frac{1}{\sqrt{2\pi}} \int_{-\infty}^{\infty} d\omega e^{-i\omega(t-t_0)} b_0(\omega). \quad (3.7)$$

With this definition in mind we carry out an integral of $b(\omega)$ over ω, yielding

$$\begin{aligned} \frac{1}{\sqrt{2\pi}} \int d\omega b(\omega) &= \frac{1}{\sqrt{2\pi}} \left(\int e^{-i\omega(t-t_0)} b_0(\omega) d\omega + \int \sqrt{\frac{\gamma}{2\pi}} \int_{t_0}^{t} e^{-i\omega(t-t_0)} a(t') dt' d\omega \right) = \\ &= b_{\text{in}}(t) + \frac{\sqrt{\gamma}}{2} a(t), \end{aligned} \quad (3.8)$$

where we have used the identities

$$\begin{cases} \int_{-\infty}^{\infty} e^{i\omega(t-t')} d\omega = 2\pi\delta(t - t') \\ \int_{t_0}^{t} a(t')\delta(t - t') dt' = \frac{1}{2} a(t). \end{cases} \quad (3.9)$$

An alternative solution to the Heisenberg equation of motion is to introduce the final state operator $b_1(\omega) = b(\omega, t = t_1)$. This lets us find a solution

$$b(\omega) = e^{-i\omega(t-t_0)} b_1(\omega) - \kappa(\omega) \int_{t_0}^{t} e^{-i\omega(t-t')} a(t') dt'. \quad (3.10)$$

We now define an *out-field*

$$b_{\text{out}}(t) = \frac{1}{\sqrt{2\pi}} \int d\omega e^{-i\omega(t-t_1)} b_1(\omega). \tag{3.11}$$

We integrate this, giving us

$$\frac{1}{\sqrt{2\pi}} \int d\omega b(\omega) = b_{\text{out}}(t) - \frac{\sqrt{\gamma}}{2} a(t). \tag{3.12}$$

Taking Eq. (3.8) and Eq. (3.12) together we end up with

$$b_{\text{out}}(t) = b_{\text{in}}(t) + \sqrt{\gamma} a(t), \tag{3.13}$$

called an input-output relation. Here, we identify $b_{\text{in}}(t)$ as corresponding to an incoming field, and $b_{\text{out}}(t)$ as corresponding to an output field. This can be done with more general system Hamiltonians, in particular the system annihilation operator a can be replaced by a more general operator, and the exact form of the Hamiltonian need not be specified.

3.1.1 SLH formalism

The SLH formalism [43] is a powerful tool for simplifying complex networks consisting of many parts which can be modelled individually. The general idea of the formalism is that if one can find the triplet (S, L, H) for any given subsystem, and from there find input-output relations for the entire network as seen above. The triplet consists of the internal scattering operator S, the loss operator L, coupling to external modes of the bath, and H, the network Hamiltonian. Both S and L correspond to scattering in some sense, the scattering operator corresponds to scattering a signal from one of the systems internal modes to another one, and our loss operator L corresponds to interaction with the environment, i.e. scattering into an external mode. Note that both S and L can consist of several scattering or loss channels, thus a vector notation is oftentimes used.

The criterion for applying the SLH formalism is that the conditions for the Markov approximation are fulfilled, as well as the assumption that all components are weakly coupled. It is derived from stochastic calculus, which we won't go into detail about. The main idea is that one can define a infinitesimal change of the time evolution unitary, which can be generalized to networks of arbitrary size and coupling topology. Rather than using these infinitesimal time steps to solve the full dynamics of the system, the SLH formalism offers a way to combine the SLH triplets of different subsystems into one triplet that describes the full system. To do this there are composition rules that can be used, these are listed here without proof. For an extensive review of the formalism, see [43].

3.1.1.1 Composition rules

Series product: The series product or cascade rule is used for connecting two subsystems 1 and 2, where the output of system 1 will pass as an input into system

2. Mathematically, one writes

$$(\boldsymbol{S}_2, \boldsymbol{L}_2, H_2) \triangleleft (\boldsymbol{S}_1, \boldsymbol{L}_1, H_1) = \left(\boldsymbol{S}_2\boldsymbol{S}_1, \boldsymbol{L}_2 + \boldsymbol{S}_2\boldsymbol{L}_1, H_1 + H_2 + \frac{1}{2i}\left(\boldsymbol{L}_2^\dagger \boldsymbol{S}_2 \boldsymbol{L}_1 - \boldsymbol{L}_1^\dagger \boldsymbol{S}_2^\dagger \boldsymbol{L}_2 \right) \right). \tag{3.14}$$

Concatenation product: The concatenation product is a way of combining two elements that are in parallel. One writes

$$(\boldsymbol{S}_1, \boldsymbol{L}_1, H_1) \boxplus (\boldsymbol{S}_2, \boldsymbol{L}_2, H_2) = \left(\begin{bmatrix} \boldsymbol{S}_1 & 0 \\ 0 & \boldsymbol{S}_2 \end{bmatrix}, \begin{bmatrix} \boldsymbol{L}_1 \\ \boldsymbol{L}_2 \end{bmatrix}, H_1 + H_2 \right). \tag{3.15}$$

Direct coupling: This is a generalization of the concatenation product, where we have two elements that are in parallel, but that are also coupled via some interaction Hamiltonian. We get

$$(\boldsymbol{S}_1, \boldsymbol{L}_1, H_1 + H_{\text{int}}) \boxplus (\boldsymbol{S}_2, \boldsymbol{L}_2, H_2) = \left(\begin{bmatrix} \boldsymbol{S}_1 & 0 \\ 0 & \boldsymbol{S}_2 \end{bmatrix}, \begin{bmatrix} \boldsymbol{L}_1 \\ \boldsymbol{L}_2 \end{bmatrix}, H_1 + H_2 + H_{\text{int}} \right). \tag{3.16}$$

3.1.2 Input-Output with pulses of radiation

In certain cases, we want to work only with pulses of radiation rather than continuous inputs and outputs. A way to do this was presented by Kiilerich and Mølmer [5, 6]. The basic principle is to consider a system where input and output are modeled with leaking virtual cavities. This means that instead of treating the system as connected to an infinite bath, it is connected to virtual cavities that leaks signals into it, and on the other side connected to cavities which the system outputs are leaked into. This is a *cascaded system*, meaning that the input cavities only send signals to the system, while the reverse direction is not allowed. These are referred to as *upstream cavities*. By the same principle the cavities that the system leaks signals into are called *downstream cavities*. This modeling of our open system lets us utilize the SLH formalism and (3.13) in order to describe the output states. For now, we will consider a system with one upstream and one downstream cavity, see Fig. 3.1. We define the time-independent creation operator

$$b_u^\dagger = \int dt u(t) b^\dagger(t), \tag{3.17}$$

since the upstream cavity only has one excitation in the mode with shape $u(t)$, so this operator is the total excitation entering the system.

We now consider the coupling between the upstream cavity and the system, which we denote $g_u(t)$. We define this as

$$g_u(t) = \frac{u^*(t)}{\sqrt{1 - \int_0^t dt' \, |u(t')|^2}}, \tag{3.18}$$

and for the downstream cavity we define

$$g_v(t) = -\frac{v^*(t)}{\sqrt{\int_0^t dt' |v(t')|^2}}, \tag{3.19}$$

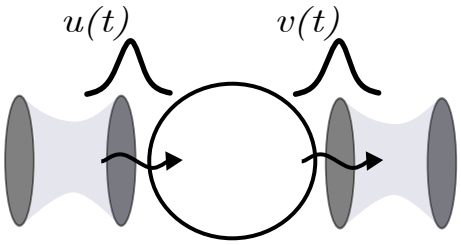

Fig. 3.1: Simple case of our model, showing how we deal with one input and one output signal entering the system with pulse shape $u(t)$ and exiting the system with pulse shape $v(t)$. This is modelled as one upstream cavity leaking its signal content to the system with coupling strength $g_u(t)$, which is then scattered into the downstream cavity with coupling strength $g_v(t)$. This model can easily be extended by regarding several inputs and outputs, which will correspond to more cavities in our model.

where $g_v(t)$ is the coupling strength between system and downstream cavity, and $v(t)$ is the envelope for the signal sent from the system. The reasoning behind these definitions is that the upstream cavity should start releasing the signal at our initial time, and that the downstream cavity should absorb the signal from the system as our time increases (asymptotically).

We have now defined a system with three network elements, the upstream cavity U, the system S and the downstream cavity D. This makes it possible to utilize the SLH formalism. In order to do this we must find the SLH triplets of our three network components. We can argue that none of our components contains internal scattering, so the S-matrix is unity for all cases. Knowing the cascaded nature of the total system, as well as assuming that the system has one loss channel, photon loss, with rate $\sqrt{\gamma}$, we can write the SLH triplets as

$$G_u = (\mathbb{1}, g_u^* a_u, \mathcal{H}_\mathrm{u}) \tag{3.20}$$
$$G_s = (\mathbb{1}, \sqrt{\gamma} a, \mathcal{H}_\mathrm{s}) \tag{3.21}$$
$$G_v = (\mathbb{1}, g_v^* a_v, \mathcal{H}_\mathrm{d}), \tag{3.22}$$

where a is a system operator corresponding to losing an excitation to the bath, a_u and a_v are operators for upstream and downstream respectively.

This now gives us the following triplet for the full system

$$G_{USD} = G_d \triangleleft G_s \triangleleft G_u. \tag{3.23}$$

Explicit evaluation gives us that

$$\begin{aligned}
&G_\mathrm{USD} = (\mathbb{1}, g_v^* a_v, \mathcal{H}_\mathrm{d}) \triangleleft \left(\mathbb{1}, \sqrt{\gamma} a + g_i^* a_u, \mathcal{H}_\mathrm{s} + \mathcal{H}_\mathrm{u} + \frac{1}{2i}\left(\sqrt{\gamma} a^\dagger g_u^* a_u - g_u a_u^\dagger \sqrt{\gamma} a\right)\right) = \\
&\Big(\mathbb{1}, g_v^* a_v + \sqrt{\gamma} a + g_u^* a_u, \mathcal{H}_\mathrm{d} + \mathcal{H}_\mathrm{s} + \mathcal{H}_\mathrm{u} + \\
&\frac{1}{2i}\left(\sqrt{\gamma} g_u^* a^\dagger a_u - \sqrt{\gamma} g_u a_u^\dagger a + g_v a_v^\dagger \left(\sqrt{\gamma} a + g_u^* a_u\right) - \left(\sqrt{\gamma} a^\dagger + g_u a_u^\dagger\right) g_v^* a_v\right)\Big) = \\
&\left(\mathbb{1}, g_v^* a_v + \sqrt{\gamma} a + g_u^* a_u, \mathcal{H}_\mathrm{d} + \mathcal{H}_\mathrm{s} + \mathcal{H}_\mathrm{u} + \frac{i}{2}\left(g_u \sqrt{\gamma} a_u^\dagger a + g_v^* \sqrt{\gamma} a^\dagger a_v + g_u g_v^* a_u^\dagger a_v - \mathrm{H.C.}\right)\right)
\end{aligned} \tag{3.24}$$

Given that we do not interest ourselves in the exact form of the cavities, since they are virtual, we neglect these terms to focus on the physical ones. This leaves us with

$$\mathcal{H}_{\text{USD}} = \mathcal{H}_{\text{s}} + \frac{i}{2}\left(g_u\sqrt{\gamma}a_u^\dagger a + g_v^*\sqrt{\gamma}a^\dagger a_v + g_u g_v^* a_u^\dagger a_v - \text{H.C.}\right). \tag{3.25}$$

An important step of this calculation is the associativity of the series product, which is easy to show by calculating $(G_1 \triangleleft G_2) \triangleleft G_3$ and $G_1 \triangleleft (G_2 \triangleleft G_3)$ for some general $G_i = (S_i, L_i, H_i)$ and seeing that they are the same.

In many cases, the system will contain more than one input or output mode. If the system is non-linear, it can be expected that the output will be released into several different modes of the output field [2]. For the purposes of information transfer, it is then important to scatter as much of the desired pulse into the same mode as possible, since one can usually assume that only one mode can be measured in the receiver. The way to measure the occupancy of each mode is through use of the auto-correlation function of the output field, calculated through use of the quantum regression theorem

$$\begin{gathered} g^{(1)}(t,t') = \langle (L_{US}(t))^\dagger L_{US}(t')\rangle = \\ \text{Tr}\left[(L_{US}(t))^\dagger U(t,t')\left(L_{US}(t)U(t',0)\rho_{US}(0)\right)\right], \end{gathered} \tag{3.26}$$

where L_{US} is the loss operator for the joint system consisting of the upstream cavity and our system, (we assume we only have one), $U(t_2,t_1)$ is the time evolution operator evolving the state from time t_1 to time t_2, and $\rho_{US}(0)$ is our initial state of the joint system [6]. The two-time correlation function has the eigenmode decomposition

$$g^{(1)}(t,t') = \sum_i n_i v_i^*(t) v_i(t'), \tag{3.27}$$

where n_i is the photon occupancy of mode i, and $v_i(t)$ is, like before, the pulse shape of the pulse leaving the system and entering the downstream cavity. This gives us a way to find the most occupied state. With this information, the coupling to the downstream virtual cavities with the correct modes can be found, from which we calculate the shape of the output pulses. Now, finally, we have a description from an arbitrary number of inputs to the system, scattering on an arbitrary system into modes with given pulse shapes.

3.2 Release of GKP states

Instead of generating a stationary GKP state in a system, it is interesting to see how the same techniques could be used to create traveling GKP states. The main idea is to combine the methods from Section 2.5 and Section 3.1.

First of all, we want a pulsed emission, so we should change the drive amplitude $A(t)$ from a sigmoid. We use $A(t) = \sin^2(\pi t/t_f)$, where t_f is the final preparation time for the state. Even after changing the drive to a pulsed signal, the frequency is still tuned by a sigmoid, as described in Section 2.5.3.

Instead of dealing with an upstream cavity, a system and a downstream cavity, we model the input to the system by making our Hamiltonian time dependent,

rather than having an upstream cavity. This leaves us with only our system, in which state preparation is handled, and a downstream cavity, modeling the most populated mode of the output field. Given that we have a system Hamiltonian Eq. (2.49), we can find the SLH triplets for both subsystems. We get

$$G_{\text{system}} = \left(\mathbb{1}, \sqrt{\gamma}a, \omega_0 a^\dagger a - Jf(t)\cos(2\sqrt{\pi}\hat{x})\right) \tag{3.28}$$

$$G_{\text{downstream}} = (\mathbb{1}, g_v^*(t)a_v, \mathcal{H}_{\text{D}})\,. \tag{3.29}$$

Using Eq. (3.14) we can find the total network loss operator and Hamiltonian. We get

$$L_{\text{tot}} = \sqrt{\gamma}a + g_v^*(t)a_v \tag{3.30}$$

$$\mathcal{H}_{\text{tot}} = \omega_0 a^\dagger a - Jf(t)\cos(2\sqrt{\pi}\hat{x}) + \frac{\sqrt{\gamma}}{2i}\left(g_v(t)a_v a^\dagger - g_v^*(t)a a_v^\dagger\right), \tag{3.31}$$

where we have once again disregarded $\mathcal{H}_{\text{D}}$.

3.3 Shortcuts to adiabaticity

In order to have controlled state evolution, there is a need for adiabatic evolution, as mentioned earlier. However, this can lead to very long preparation times, which is problematic since this allows losses to act for longer. Therefore, many applications need a way to speed up the state generation process while still yielding the same state as the adiabatic protocol. The set of methods doing this are referred to as shortcuts to adiabaticity (STA) [35, 37, 44].

On such method is through adding a *counter-diabatic* term. Assume, as before, that we have an adiabatic Hamiltonian $\mathcal{H}_{\text{ad}}(t)$, fulfilling the Schrödinger equation

$$\mathcal{H}_{\text{ad}}(t)\left|n(t)\right\rangle = E_n(t)\left|n(t)\right\rangle, \tag{3.32}$$

where $|n(t)\rangle$ are the eigenstates of the adiabatic Hamiltonian. We know that the Schrödinger equation for our adiabatic Hamiltonian is $\mathcal{H}_{\text{ad}}(t)\left|n(t)\right\rangle = i\partial_t\left|n(t)\right\rangle$ and that its formal solution is

$$\left|\psi_n(t)\right\rangle = e^{i\xi_n(t)}\left|n(t)\right\rangle. \tag{3.33}$$

Now, let us assume that there is an additional Hamiltonian $\mathcal{H}(t)$ that fulfills this Schrödinger equation, i.e.

$$\mathcal{H}(t)\left|\psi_n(t)\right\rangle = i\partial_t\left|\psi_n(t)\right\rangle, \tag{3.34}$$

where we now want to solve for this new Hamiltonian. It can then be shown [35] that the Hamiltonian will be on the form

$$\mathcal{H}(t) = \sum_n E_n(t)\left|n(t)\right\rangle\left\langle n(t)\right| + i\sum_n \left(\mathbb{1} - \left|n(t)\right\rangle\left\langle n(t)\right|\right)\partial_t\left|n(t)\right\rangle\left\langle n(t)\right|. \tag{3.35}$$

We can identify the first term as our adiabatic Hamiltonian $\mathcal{H}_{\text{ad}}(t)$, while the second term is referred to as the *counter-diabatic* term, $\mathcal{H}_{\text{cd}}$, i.e.

$$\mathcal{H}(t) = \mathcal{H}_{\text{ad}} + \mathcal{H}_{\text{cd}}. \tag{3.36}$$

$\mathcal{H}_{\mathrm{cd}}(t)$ can be written as ([37])

$$\mathcal{H}_{\mathrm{cd}}(t) = i \sum_{m \neq n} \frac{\langle m(t)|(\partial_t \mathcal{H}_{\mathrm{ad}}(t))|n(t)\rangle}{E_n(t) - E_m(t)} |m(t)\rangle \langle n(t)| . \tag{3.37}$$

This is in the case of no degeneracies of the eigenvalues. In the case of degeneracy, the counter-diabatic term can be modified to exclude summation with two equal eigenenergies. This is done by adding another index to the state, which orders the degenerate states. The counter-diabatic term with degeneracies is written as

$$\mathcal{H}_{\mathrm{cd}}(t) = i \sum_{\substack{m \neq n \\ \mu \neq \nu}} \frac{\langle m(t), \mu|(\partial_t \mathcal{H}_{\mathrm{ad}}(t))|n(t), \nu\rangle}{E_{n,\nu}(t) - E_{m,\mu}(t)} |m(t), \mu\rangle \langle n(t), \nu| . \tag{3.38}$$

4

Results and discussion

In this chapter we present and discuss the results from simulated preparation of GKP states. We begin with closed system generation of GKP states, from which we add the counter-diabatic term and open the system, while studying the multimodeness. After this we employ the full system-downstream Hamiltonian to catch the most populated state in the output field.

For our model, we will assume a constant resonance frequency ω_0 in our system, which we set to be a standard harmonic oscillator when driving is absent. In a superconducting circuit setting, ω_0 would be in the range of a few GHz. We define the time scale in relation to this frequency as $T = 2\pi/\omega_0$. This is the period time of our Floquet Hamiltonian, and our total preparation time should be an integer multiple of T in order to get the correct Floquet dynamics, as stated in Section 2.5.3. We will restrict ourselves to dealing with preparation of $|+\rangle_{\text{GKP}}$ states. This is because in our open system settings, we will have a very strong coupling to the environment, and we will therefore rapidly lose the $|2\rangle$ initial state that is necessary for preparation of $|-\rangle_{\text{GKP}}$. The preparation scheme of this thesis will have to be further developed in order to prepare $|-\rangle_{\text{GKP}}$ states.

4.1 Generation of stationary GKP states

The first crucial step of releasing GKP states into a waveguide is to first be able to deterministically prepare stationary GKP states in our circuit. Following the procedure of [1], the Hamiltonian Eq. (2.27) with the drive Eq. (2.50) is implemented. This is simulated in a closed system with a system dimension of 30. We choose to start with a preparation time $t_f = 600T$. First, we generate the states with a sigmoid drive, choosing the drive strength $J = 0.00125\,\omega_0$. The Wigner plots of generated $|+\rangle_{\text{GKP}}$ and $|-\rangle_{\text{GKP}}$ states is shown in Fig. 4.1a.

Given the limitations on the dimensionality, as well as approximations like the truncation of the Fourier series of our delta peaks, this does indeed look like a GKP-like state, and shows that we have a working implementation of [1]. However, to emit a single pulse, we should change the preparation scheme such that the sigmoidal ramp is replaced by a pulsed envelope. We choose a $\sin^2$ pulse, i.e. $A(t) = \sin^2(\pi t/t_f)$. Given that this pulse shape decreases the drive function overall, we also need to find a suitable value for the drive strength J. This new value is chosen to be $J = 0.005\,\omega_0$, i.e. four times higher drive strength, and the corresponding circuit Wigner functions are shown in Fig. 4.1b.

The quality of this state has decreased due to the change of the drive function.

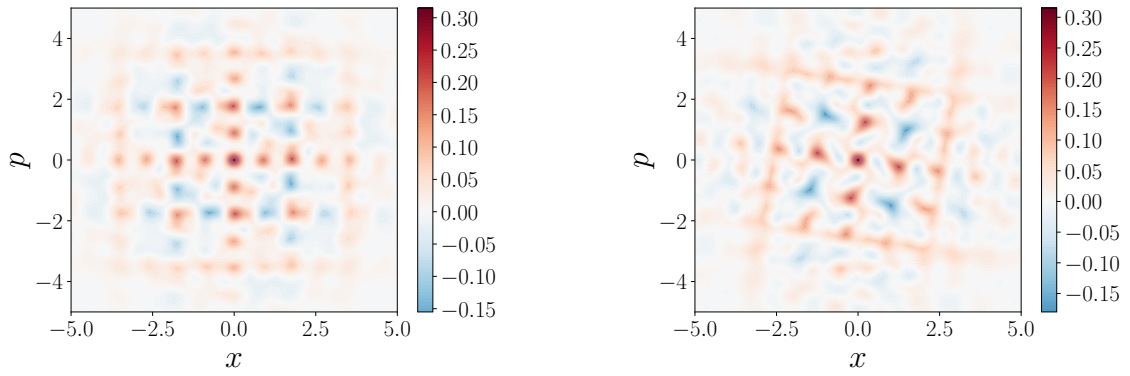

(a) **(b)**

Fig. 4.1: Stationary $|+\rangle_{\mathrm{GKP}}$ shown in (a) [(b)] with $n = 6.40$ ($n = 6.29$) simulated in a closed system with $J = 0.00125\,\omega_0$. The drive is a sigmoid ramp ($\sin^2$). In both cases, we see a grid like structure with positive and negative contributions, as expected for GKP-like states. We note that changing the envelope shape affects the distribution of positive and negative peaks, while still keeping a grid structure.

We can see that the Wigner negativity of the state is distributed differently, even disregarding linear transformations, and also that the localized points are more spread out. This is not ideal, and could definitely be optimized for better fidelity with the previous state. This could be a future improvement, but is currently insignificant in comparison to getting a downstream state population, and is therefore disregarded for the remainder of this work. We will also see that subsequent steps of state generation will affect the state more severely.

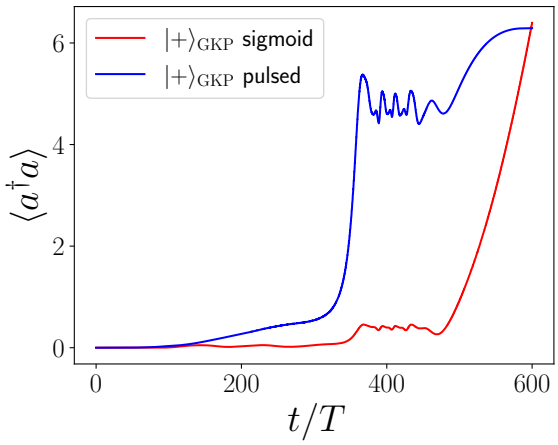

Fig. 4.2: Photon numbers as a function of time for the two prepared states in Fig. 4.1a (red) and Fig. 4.1b (blue). The difference between sigmoid and pulsed drive has a clear impact of the photon number in the system.

The photon numbers of the prepared states during the preparation is shown in Fig. 4.2. The differences between the two types of drive becomes very clear. Since we have different preparation schemes, it is very reasonable that we end up with different states in the two cases. However, they are still GKP like, with focused

points of Wigner state population, positive and negative interspersed.

4.2 Shortcuts to adiabaticity

In order to have faster state preparation and release, we implement the counter-diabatic term discussed in Section 3.3.

The purpose of adding the counter-diabatic term is to lower the preparation time, so we now change it to $t_f = 150\,T$, and then try to replicate the pulsed drive state generation that we have seen before. We choose the drive strength value $J \approx 0.002\,\omega_0$. The corresponding Wigner function is shown in Fig. 4.3, with photon numbers in Fig. 4.4.

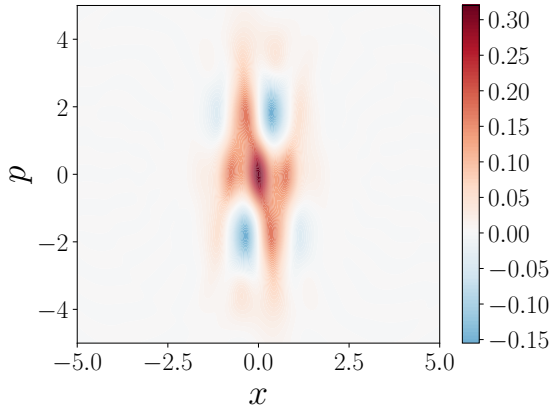

Fig. 4.3: Closed system generation of $|+\rangle_{\mathrm{GKP}}$ with counter-diabatic term and $J \approx 0.002\,\omega_0$. The photon count is $n = 1.68$, and the drive envelope is a $\sin^2$ pulse. This state is largely different from previous GKP states, but still contains large Wigner negative sections, and carry a resemblance to squeezed cat states.

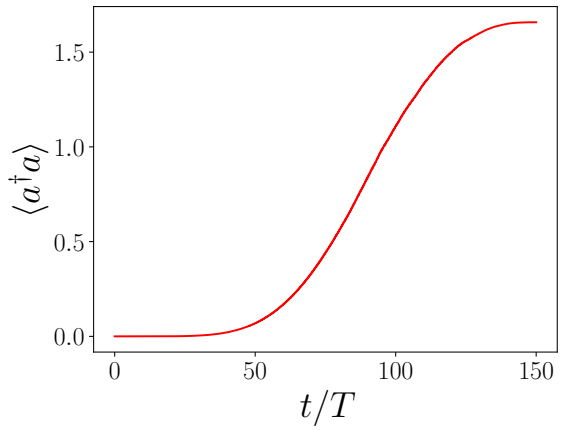

Fig. 4.4: Photon number over time for $|+\rangle_{\mathrm{GKP}}$ as seen in Fig. 4.3. We see that the intermediate photon number changes in a slow fashion, with the final photon numbers being in a reasonable range for GKP states.

We see that this state is severely affected by the addition of the counter-diabatic term. Ideally, this should not happen, since the GKP states are eigenstates of the GKP Hamiltonian Eq. (2.27), and the counter-diabatic term should perserve the eigenvalues. It is likely that this doesn't hold for our system, since the drive in our adiabatic term consists of a sum of cosines. When finding the counter-diabatic term, the time derivative of the adiabatic term is used. This will result in a sum of sines, corresponding to the Fourier series of another set of delta peaks shifted in time by $T/2$. These changes to the Hamiltonian are quite drastic, and could clash with the assumptions of our counter-diabatic term. Improving this is another subject for future research.

4.3 Open system and correlation functions

All previous results are for a closed system setting. We open the system and implement Eq. (3.30) with a constant coupling strength $\gamma \approx 0.019\,\omega_0$. Since we aim to leak the state, it is no longer relevant to look at the Wigner function in the system, rather it's the output field state information we seek.

The simulations in this, and next, section are carried out with a system dimension of 15, since we will not populate as high levels with photon loss present. We pick a drive strength $J = 0.0048\,\omega_0$ and the preparation time $t_f = 240\,T$. It is clear that we are in a very strong coupling regime, since $\gamma = 4J$. It is important to make sure that we release the entire state, since residual photon content in the system will be entangled with the downstream, and can give more multimode behaviour. Now, the photon number is approximately zero at t_f, as seen in Fig. 4.5.

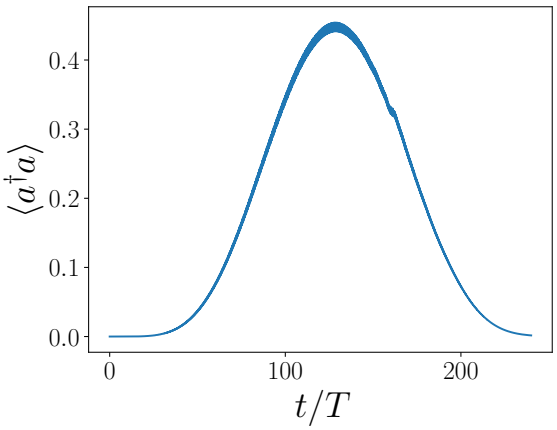

Fig. 4.5: Photon number for preparation of $|+\rangle_{\text{GKP}}$ with $\gamma = 0.019\,\omega_0$. Note that the photon number at the final time is close to zero, meaning that almost everything has leaked out of the state. Note also that the photon number contains some fluctuations. These are likely caused by the fast oscillating term in our Hamiltonian, as well as a strong interaction with the environment.

As might be expected, we have very much lower system population due to the strong coupling, even at the maximum, only reaching about 0.45 photons.

Knowing that the entire state is released, we can find the full photon count of the output field (i.e. sum of all output modes) as

$$n_{\text{output}} = \int dt \, \langle L^\dagger L \rangle = \int dt \gamma \, \langle a^\dagger a \rangle \, , \tag{4.1}$$

and in this case get $n_{\text{output}} = 5.05$, which is in our higher limit of reasonable values for implementable GKP.

As stated in Eq. (3.27), it should be possible to calculate the photon number by calculating the two-time two-operator correlation function $g^{(1)}(t, t')$. This correlation function contains a lot of fluctuations, which affects these calculations. One possible reason for this is that since the Hamiltonian has a lot of sudden peaks, so does the correlation function, and by extension both its eigenvalues (the photon numbers in each mode) and eigenfunctions (our temporal modes) get unphysical sudden jumps. This is especially clear in the eigenfunctions, which will yield time dependent coupling strengths $g_v(t)$ that do not correspond to catching a physical mode, leading to no population of the corresponding virtual cavity.

Since we cannot rely on the fluctuating decomposition as is, we will remove the fluctuations in our $v_i(t)$ by a simple moving average in order to smooth the pulses out. This approximation allows us to extract temporal envelopes that we can use for the remainder of the preparation scheme. We use these pulses in order to extract our virtual coupling strength $g_v(t)$. We can assume that this approximation results in some redistribution of photons between modes. The magnitude of the errors from smoothing the wave-packets is currently unknown, but they are expected to be quite small since we only smooth sudden changes in the pulses, and, as mentioned, state emission is inhibited if the smoothing is not performed. Ideally, this would be the subject of future research.

4.4 Full system

We simulate the full system-downstream network with our full Hamiltonian containing the counter-diabatic term. In these simulations we have a considerably shorter preparation time compared to the closed system. We choose a preparation time $t_f = 50\,T$ and a drive strength $J = 0.008\,\omega_0$. We see the two most populated modes in Fig. 4.6, with the photon number of the most populated mode in Fig. 4.7. It is important to note that the photon count in the system at the final preparation time is non-zero. As mentioned before, this could mean that the residual state in the circuit could be entangled with the downstream mode. In order to mitigate this, the system is evolved past the preparation time, letting the system population decay to zero without any applied drive before observing the downstream state. The reason for this procedure is to make sure that γ determines the time frame for the preparation, rather than our preparation parameters, e.g. J or t_f. This ensures that our preparation is as fast as possible.

We have a clear difference between the two Wigner functions in Fig. 4.6, with three times higher population in the most populated mode. The most populated mode also contains Wigner negative parts, whereas the second most populated mode is strictly positive. Calculating the total photon number of the output field by

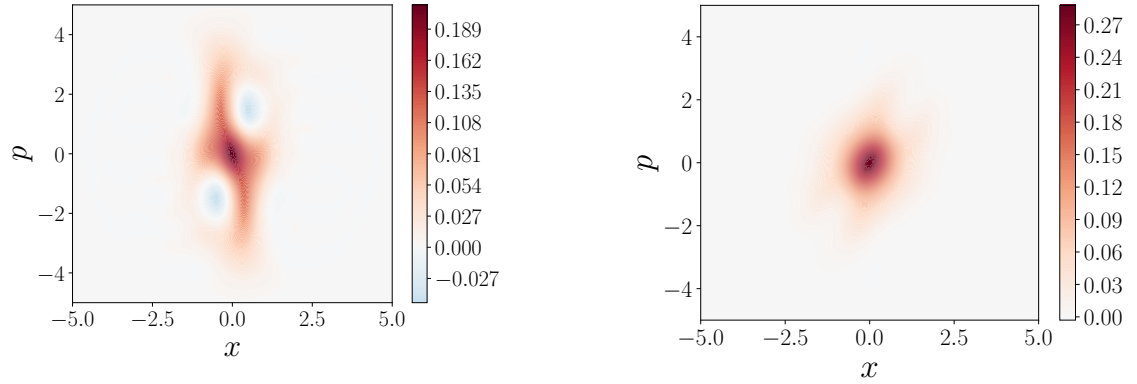

(a) **(b)**

Fig. 4.6: Wigner function of (a) the most populated mode with photon count $n_1 = 1.58$ and (b) the second most populated mode with photon count $n_2 = 0.44$ simulated with $J = 0.008\,\omega_0$ and $\gamma = 0.019\,\omega_0$. The total photon number of the output field is $n_{\text{output}} = 2.41$. We note that all negativity is located in the most populated mode.

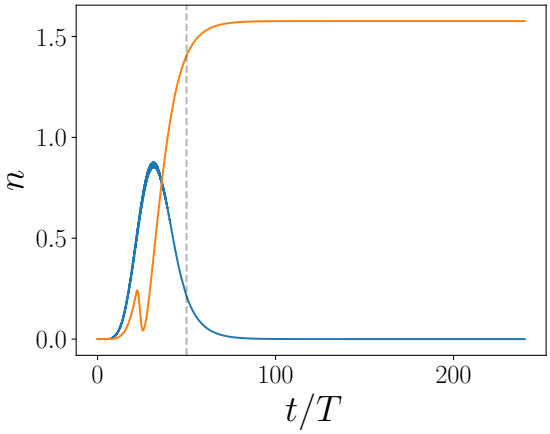

Fig. 4.7: Photon number for circuit (blue) and most populated downstream mode (orange) for the simulation shown in Fig. 4.6. We see that the downstream mode population is saturated at the final time. The behaviour at the beginning of emission is not as smooth as before, most likely a result of the counter-diabatic term adding more complexity to the correlation function.

Eq. (4.1) gives $n_{\text{output}} = 2.41$, and through adding up the 15 largest eigenvalues of Eq. (3.27) we get $n_{\text{output}} = 2.38$, with the values for the first two modes being $n_1 = 1.76$ and $n_2 = 0.37$. The discrepancy between these values and the final expectation values of Fig. 4.6 most likely originates from the eigenvalues of $g^{(1)}(t, t')$ being inexact for the same reasons the eigenfunctions get fluctuations.

We decrease the drive strength to $J = 0.005\,\omega_0$ while keeping $t_f = 50\,T$. We show the two most populated modes in Fig. 4.8. As for the previous result, this gives an overwhelming portion of the photon population located in a single mode. We also see that the most populated state is fairly similar to earlier results, except

for a linear rotation, it contains negativity and the shape is as before.

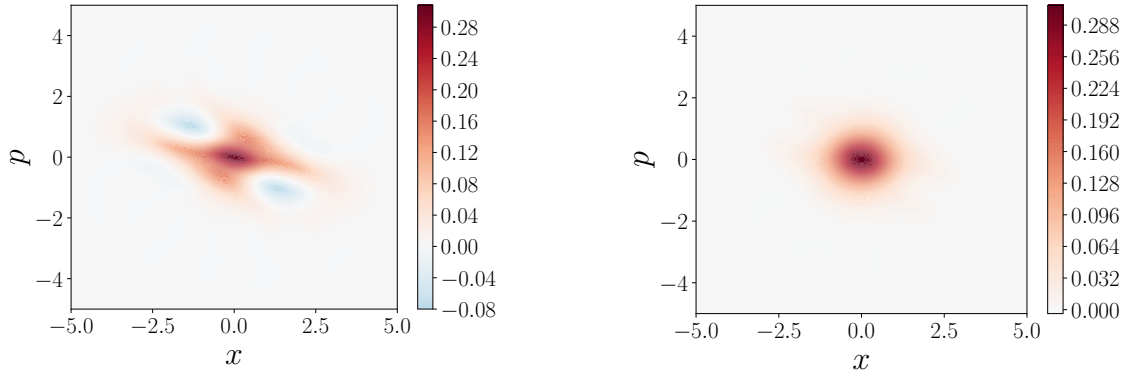

(a) **(b)**

Fig. 4.8: Wigner function of the most populated mode with photon count $n_1 = 0.78$ (a) and the second most populated mode with photon count $n_2 = 0.15$ (b). The parameter values are $J = 0.005\,\omega_0$, $t_f = 50\,T$ and $\gamma = 0.019\,\omega_0$. The total photon count of the output field is $n_{\text{output}} = 0.95$.

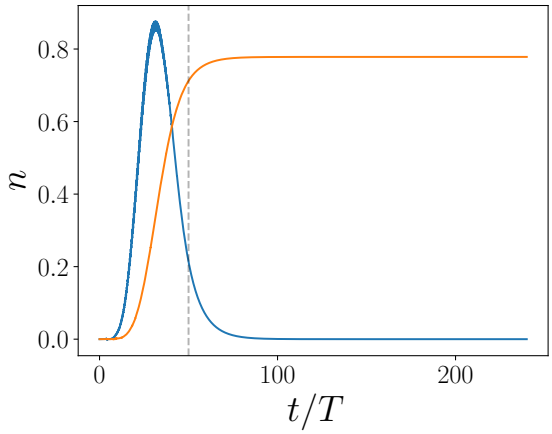

Fig. 4.9: Photon number for circuit (blue) and most populated downstream mode (orange) for the simulation in Fig. 4.8, with drive applied until $t_f = 50\,T$ with counter-diabatic time evolution. We see that the downstream mode population is saturated at the final time.

The photon counts from the expectation values during the simulations gives us $n_1 = 0.78$ and $n_2 = 0.15$, still with around three times the population in the most populated mode. Equation (4.1) gives the total photon count of the output field as $n_{\text{output}} = 0.95$. Adding the first two mode population together gives 0.93, which is less than the total of 0.95, albeit with small marginal for the populations in the remaining modes. It is also interesting to note that the mode population calculated with Eq. (3.27) gives $n_1 = 0.71$ and $n_2 = 0.13$, which is quite close to our result, with the discrepancy most likely coming from the fluctuations of the auto-correlation function as before.

We note that the state in Fig. 4.8a is somewhat similar to a squeezed cat state. These states are defined through the expression

$$|\psi_{\text{sq. cat}}\rangle = S_r(\theta)\left(D(\alpha) + D(-\alpha)\right)|0\rangle\,, \tag{4.2}$$

with $S_r(\theta)$ being the squeeze operator, squeezing the state with the squeezing parameter r along an axis defined by θ, and $D(\alpha)$ being the displacement operator displacing the state by $\alpha \in \mathbb{C}$ in phase space. These operators are defined as

$$S_r(\theta) = \exp\left(\frac{r}{2}\left(e^{-i\theta}a^2 - e^{i\theta}a^{\dagger 2}\right)\right) \tag{4.3}$$

$$D(\alpha) = \exp\left(\alpha a^\dagger - \alpha^* a\right). \tag{4.4}$$

Through optimizing the fidelity between a squeezed cat state and the state seen in Fig. 4.8a, the squeezed cat state in Fig. 4.10. is found. The parameters found are $r = 0.44$, $\theta = 1.26$ and $\alpha = 0.89e^{0.42i}$. The fidelity between the most populated downstream mode state and this squeezed cat state is found to be 92 %.

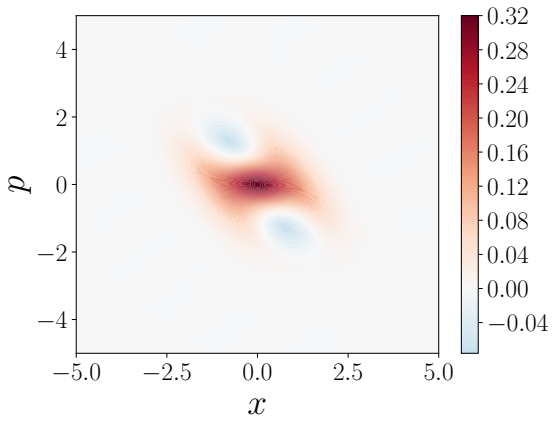

Fig. 4.10: Wigner function of squeezed cat state with maximum state overlap with Fig. 4.8a. State parameters are $r = 0.44$, $\theta = 1.26$ and $\alpha = 0.89e^{0.42i}$.

We note that the final states in the downstream modes found in this section are somewhat similar to the closed system state after applying the counter-diabatic term. We apply a linear rotation to the state in Fig. 4.8a by some angle ϕ, which we optimize to maximize fidelity between these two states. The resulting fidelity is 93 %. We see that while we would ideally be closer to 100 % in order to have useful state emission, this is still promising since we reached this value without optimization of system parameters such as J, t_f or γ. By tuning these, the fidelity might be improved.

5
Conclusion

Distributed quantum computing remains one of the most promising avenues for implementing near term quantum computers. In order to enable this, secure communication between computational devices is crucial, creating a need for error correctable flying states. One of the most prominent quantum error correction schemes available is the GKP encoding, a bosonic system code utilizing a grid-like phase space structure to encode a binary computational basis. There are ways of generating approximate GKP states such that they are stationary in a circuit.

This work aimed to generate traveling GKP states, but succeeded in the more modest goal of implementing a preparation scheme which generates somewhat interesting states, displaying negativity in the output field and carrying a resemblance to squeezed cat states, but which could certainly be improved upon to hopefully produce traveling GKP states. We have generated stationary GKP states in a system circuit, from which we have opened our system, identifying the multimode character of the emission. We have noted that the biggest issue with the current preparation is the STA, which removes the resemblance to GKP states, while the emission itself seems to work reasonably well, with room for improvement to increase the single modeness as well as the fidelity with the closed system state.

5.1 Future work

There are several extensions and improvements to be made on the scheme presented here. First of all, from the stationary generation, every subsequent step has yielded a state that looks less and less like a GKP state. Most likely, the earliest errors in the preparation propagate through subsequent steps, so by fixing them, we are more likely to release a GKP state. Some possible ways to do this is by more closely approximate the GKP Hamiltonian, for example through more terms in the Fourier series of $f(t)$, or through a more thorough analysis of how the STA:s work with our Floquet Hamiltonian.

The largest error seems to come from the STA implementation. We have seen that the closed system state after adding this term could be sent out with 93 % fidelity, meaning that if we improve this step so that we might have a GKP-like state after including STA:s, we might see GKP-like states in the downstream.

Moreover, a more thorough investigation of the parameter space is necessary, in order to have optimal preparation and release. One possible approach is through numerical optimization by maximizing the state fidelity between the traveling state and a GKP state. This is not a near term extension, since it will most likely

necessitate GKP-like states for a larger parameter space before being attempted.

Another important aspect to study is the details of the multimode distribution, as well as what steps can be taken to make it more single mode. From what we have seen we can replicate the state distribution in phase space, but with less amplitude due to the scattering. In the ideal case we would reach a method for single mode emission, after which we can expect to have successful emission.

Furthermore, an important extension would be to consider time dependent quantum control. This could affect the multimodeness of the problem, and would give more flexibility in the preparation than the static decay rate γ used in this thesis.

Bibliography

[1] X. C. Kolesnikow, R. W. Bomantara, A. C. Doherty, and A. L. Grimsmo, "Gottesman-kitaev-preskill state preparation using periodic driving," *Phys. Rev. Lett.*, vol. 132, p. 130 605, 13 Mar. 2024. DOI: 10.1103/PhysRevLett.132.130605. [Online]. Available: https://link.aps.org/doi/10.1103/PhysRevLett.132.130605.

[2] M. Khanahmadi, M. M. Lund, K. Mølmer, and G. Johansson, "Multimode character of quantum states released from a superconducting cavity," *Phys. Rev. Res.*, vol. 5, p. 043 071, 4 Oct. 2023. DOI: 10.1103/PhysRevResearch.5.043071. [Online]. Available: https://link.aps.org/doi/10.1103/PhysRevResearch.5.043071.

[3] J. Johansson, P. Nation, and F. Nori, "Qutip: An open-source python framework for the dynamics of open quantum systems," *Computer Physics Communications*, vol. 183, no. 8, pp. 1760–1772, 2012, ISSN: 0010-4655. DOI: https://doi.org/10.1016/j.cpc.2012.02.021. [Online]. Available: https://www.sciencedirect.com/science/article/pii/S0010465512000835.

[4] J. Johansson, P. Nation, and F. Nori, "Qutip 2: A python framework for the dynamics of open quantum systems," *Computer Physics Communications*, vol. 184, no. 4, pp. 1234–1240, 2013, ISSN: 0010-4655. DOI: https://doi.org/10.1016/j.cpc.2012.11.019. [Online]. Available: https://www.sciencedirect.com/science/article/pii/S0010465512003955.

[5] A. H. Kiilerich and K. Mølmer, "Input-output theory with quantum pulses," *Phys. Rev. Lett.*, vol. 123, p. 123 604, 12 Sep. 2019. DOI: 10.1103/PhysRevLett.123.123604. [Online]. Available: https://link.aps.org/doi/10.1103/PhysRevLett.123.123604.

[6] A. H. Kiilerich and K. Mølmer, "Quantum interactions with pulses of radiation," *Phys. Rev. A*, vol. 102, p. 023 717, 2 Aug. 2020. DOI: 10.1103/PhysRevA.102.023717. [Online]. Available: https://link.aps.org/doi/10.1103/PhysRevA.102.023717.

[7] R. P. Feynman, "Simulating physics with computers," *International journal of theoretical physics*, vol. 21, no. 6/7, pp. 467–488, 1982.

[8] E. Farhi, J. Goldstone, and S. Gutmann, *A quantum approximate optimization algorithm*, 2014. arXiv: 1411.4028 [quant-ph].

[9] A. F. Kockum, "Quantum optics with artificial atoms," Ph.D. dissertation, Chalmers University of Technology, 2014.

[10] J. J. Sakurai and J. Napolitano, *Modern Quantum Mechanics*, 3rd ed. Cambridge University Press, 2020.

[11] H. P. Breuer and F. Petruccione, *The theory of open quantum systems*. Great Clarendon Street: Oxford University Press, 2002.

[12] M. Kudra *et al.*, "Robust preparation of wigner-negative states with optimized snap-displacement sequences," *PRX Quantum*, vol. 3, p. 030 301, 3 Jul. 2022. DOI: 10.1103/PRXQuantum.3.030301. [Online]. Available: https://link.aps.org/doi/10.1103/PRXQuantum.3.030301.

[13] E. Wigner, "On the quantum correction for thermodynamic equilibrium," *Phys. Rev.*, vol. 40, pp. 749–759, 5 Jun. 1932. DOI: 10.1103/PhysRev.40.749. [Online]. Available: https://link.aps.org/doi/10.1103/PhysRev.40.749.

[14] A. Serafini, *Quantum Continuous Variables: A Primer of Theoretical Methods*, 1st ed. CRC Press, 2017. DOI: https://doi.org/10.1201/9781315118727.

[15] F. Quijandría, I. Strandberg, and G. Johansson, "Steady-state generation of wigner-negative states in one-dimensional resonance fluorescence," *Phys. Rev. Lett.*, vol. 121, p. 263 603, 26 Dec. 2018. DOI: 10.1103/PhysRevLett.121.263603. [Online]. Available: https://link.aps.org/doi/10.1103/PhysRevLett.121.263603.

[16] K. Kleinbeck, H. Busche, N. Stiesdal, S. Hofferberth, K. Mølmer, and H. P. Büchler, "Creation of nonclassical states of light in a chiral waveguide," *Phys. Rev. A*, vol. 107, p. 013 717, 1 Jan. 2023. DOI: 10.1103/PhysRevA.107.013717. [Online]. Available: https://link.aps.org/doi/10.1103/PhysRevA.107.013717.

[17] A. Mari and J. Eisert, "Positive wigner functions render classical simulation of quantum computation efficient," *Phys. Rev. Lett.*, vol. 109, p. 230 503, 23 Dec. 2012. DOI: 10.1103/PhysRevLett.109.230503. [Online]. Available: https://link.aps.org/doi/10.1103/PhysRevLett.109.230503.

[18] V. Veitch, C. Ferrie, D. Gross, and J. Emerson, "Negative quasi-probability as a resource for quantum computation," *New Journal of Physics*, vol. 14, no. 11, p. 113 011, Nov. 2012. DOI: 10.1088/1367-2630/14/11/113011. [Online]. Available: https://dx.doi.org/10.1088/1367-2630/14/11/113011.

[19] C. Gerry and P. Knight, *Introductory Quantum Optics*. Cambridge University Press, 2004.

[20] I. Strandberg, *Quantum state tomography of 1d resonance fluorescence*, 2017.

[21] T. Curtright, D. Fairlie, and C. Zachos, *A Concise Treatise on Quantum Mechanics in Phase Space*. Dec. 2016, ISBN: ISBN-13: 978-9814520430.

[22] M. A. Nielsen and I. L. Chuang, *Quantum Computation and Quantum Information*. Cambridge University Press, 2000, ISBN: 9781107002173.

[23] A. F. Kockum *et al.*, *Lecture notes on quantum computing*, 2024. arXiv: 2311.08445 [quant-ph].

[24] V. V. Albert and P. Faist, Eds., *The Error Correction Zoo*. 2024. [Online]. Available: https://errorcorrectionzoo.org/.

[25] D. Gottesman, A. Kitaev, and J. Preskill, "Encoding a qubit in an oscillator," *Physical Review A*, vol. 64, Sep. 2000. DOI: 10.1103/PhysRevA.64.012310.

[26] A. J. Brady, A. Eickbusch, S. Singh, J. Wu, and Q. Zhuang, "Advances in bosonic quantum error correction with gottesman–kitaev–preskill codes: Theory, engineering and applications," *Progress in Quantum Electronics*, p. 100 496, 2024, ISSN: 0079-6727. DOI: https://doi.org/10.1016/j.pquantelec.

2023.100496. [Online]. Available: https://www.sciencedirect.com/science/article/pii/S0079672723000459.

[27] A. L. Grimsmo and S. Puri, "Quantum error correction with the gottesman-kitaev-preskill code," *PRX Quantum*, vol. 2, p. 020 101, 2 Jun. 2021. DOI: 10.1103/PRXQuantum.2.020101. [Online]. Available: https://link.aps.org/doi/10.1103/PRXQuantum.2.020101.

[28] J. Hastrup and U. L. Andersen, "Protocol for generating optical gottesman-kitaev-preskill states with cavity qed," *Phys. Rev. Lett.*, vol. 128, p. 170 503, 17 Apr. 2022. DOI: 10.1103/PhysRevLett.128.170503. [Online]. Available: https://link.aps.org/doi/10.1103/PhysRevLett.128.170503.

[29] J. Hastrup, K. Park, J. B. Brask, R. Filip, and U. L. Andersen, "Measurement-free preparation of grid states," *npj Quantum Information*, vol. 7, no. 1, p. 17, Jan. 2021, ISSN: 2056-6387. DOI: 10.1038/s41534-020-00353-3. [Online]. Available: https://doi.org/10.1038/s41534-020-00353-3.

[30] R. Dahan, G. Baranes, A. Gorlach, R. Ruimy, N. Rivera, and I. Kaminer, "Creation of optical cat and gkp states using shaped free electrons," *Phys. Rev. X*, vol. 13, p. 031 001, 3 Jul. 2023. DOI: 10.1103/PhysRevX.13.031001. [Online]. Available: https://link.aps.org/doi/10.1103/PhysRevX.13.031001.

[31] S. Bravyi and A. Kitaev, "Universal quantum computation with ideal clifford gates and noisy ancillas," *Phys. Rev. A*, vol. 71, p. 022 316, 2 Feb. 2005. DOI: 10.1103/PhysRevA.71.022316. [Online]. Available: https://link.aps.org/doi/10.1103/PhysRevA.71.022316.

[32] B. Q. Baragiola, G. Pantaleoni, R. N. Alexander, A. Karanjai, and N. C. Menicucci, "All-gaussian universality and fault tolerance with the gottesman-kitaev-preskill code," *Phys. Rev. Lett.*, vol. 123, p. 200 502, 20 Nov. 2019. DOI: 10.1103/PhysRevLett.123.200502. [Online]. Available: https://link.aps.org/doi/10.1103/PhysRevLett.123.200502.

[33] B. W. Reichardt, "Quantum universality from magic states distillation applied to css codes," *Quantum Information Processing*, vol. 4, no. 3, pp. 251–264, Aug. 2005, ISSN: 1573-1332. DOI: 10.1007/s11128-005-7654-8. [Online]. Available: https://doi.org/10.1007/s11128-005-7654-8.

[34] T. Albash and D. A. Lidar, "Adiabatic quantum computation," *Reviews of Modern Physics*, vol. 90, no. 1, Jan. 2018, ISSN: 1539-0756. DOI: 10.1103/revmodphys.90.015002. [Online]. Available: http://dx.doi.org/10.1103/RevModPhys.90.015002.

[35] M. Nakahara, "Counterdiabatic formalism of shortcuts to adiabaticity," *Philosophical Transactions of the Royal Society A: Mathematical, Physical and Engineering Sciences*, vol. 380, no. 2239, p. 20 210 272, 2022. DOI: 10.1098/rsta.2021.0272. eprint: https://royalsocietypublishing.org/doi/pdf/10.1098/rsta.2021.0272. [Online]. Available: https://royalsocietypublishing.org/doi/abs/10.1098/rsta.2021.0272.

[36] M. V. Berry, "Quantal phase factors accompanying adiabatic changes," *Proceedings of the Royal Society of London. Series A, Mathematical and Physical Sciences*, vol. 392, no. 1802, pp. 45–57, 1984, ISSN: 00804630. [Online]. Available: http://www.jstor.org/stable/2397741 (visited on 05/03/2024).

[37] T. Hatomura, "Shortcuts to adiabatic cat-state generation in bosonic josephson junctions," *New Journal of Physics*, vol. 20, no. 1, p. 015 010, Jan. 2018. DOI: 10.1088/1367-2630/aaa117. [Online]. Available: https://dx.doi.org/10.1088/1367-2630/aaa117.

[38] F. Haake, "Quantum signatures of chaos," in *Quantum Coherence in Mesoscopic Systems*, B. Kramer, Ed. Boston, MA: Springer US, 1991, pp. 583–595, ISBN: 978-1-4899-3698-1. DOI: 10.1007/978-1-4899-3698-1_38. [Online]. Available: https://doi.org/10.1007/978-1-4899-3698-1_38.

[39] N. Tsuji, "Floquet states," in *Encyclopedia of Condensed Matter Physics*. Elsevier, 2024, pp. 967–980, ISBN: 9780323914086. DOI: 10.1016/b978-0-323-90800-9.00241-9. [Online]. Available: http://dx.doi.org/10.1016/B978-0-323-90800-9.00241-9.

[40] W. Pfaff *et al.*, "Controlled release of multiphoton quantum states from a microwave cavity memory," *Nature Physics*, vol. 13, no. 9, pp. 882–887, Sep. 2017, ISSN: 1745-2481. DOI: 10.1038/nphys4143. [Online]. Available: https://doi.org/10.1038/nphys4143.

[41] C. J. Axline *et al.*, "On-demand quantum state transfer and entanglement between remote microwave cavity memories," *Nature Physics*, vol. 14, no. 7, pp. 705–710, Jul. 2018, ISSN: 1745-2481. DOI: 10.1038/s41567-018-0115-y. [Online]. Available: https://doi.org/10.1038/s41567-018-0115-y.

[42] C. W. Gardiner and M. J. Collett, "Input and output in damped quantum systems: Quantum stochastic differential equations and the master equation," *Phys. Rev. A*, vol. 31, pp. 3761–3774, 6 Jun. 1985. DOI: 10.1103/PhysRevA.31.3761. [Online]. Available: https://link.aps.org/doi/10.1103/PhysRevA.31.3761.

[43] J. K. Joshua Combes and M. Sarovar, "The SLH framework for modeling quantum input-output networks," *Advances in Physics: X*, vol. 2, no. 3, pp. 784–888, 2017. DOI: 10.1080/23746149.2017.1343097. eprint: https://doi.org/10.1080/23746149.2017.1343097. [Online]. Available: https://doi.org/10.1080/23746149.2017.1343097.

[44] K. Takahashi, "Transitionless quantum driving for spin systems," *Phys. Rev. E*, vol. 87, p. 062 117, 6 Jun. 2013. DOI: 10.1103/PhysRevE.87.062117. [Online]. Available: https://link.aps.org/doi/10.1103/PhysRevE.87.062117.

DEPARTMENT OF MICROTECHNOLOGY AND NANOSCIENCE
CHALMERS UNIVERSITY OF TECHNOLOGY
Gothenburg, Sweden
www.chalmers.se

CHALMERS
UNIVERSITY OF TECHNOLOGY